into acute anemia rat model. Biomaterials 2006;27:4477-4483.
33. Komatsu T, Ohmichi N, Zunszain PA, Curry S, Tsuchida E. Dioxygenation of human serum albumin having a prosthetic heme group in a tailor-made heme pocket. J Am Chem Soc 2004;126:14304-14305.
34. Paoli M. Anderson BF, Baker HM, Morgan WT, Smith A, Baker EN. Crystal structure of hemopexin reveals a novel high-affinity heme site formed between two β-propella domains. Nat Struct Biol 1999;6:926-931.
35. Fairley NH. Methemalbumin (pseudo-methemoglobin). Nature 1938;142:1156-1157.
36. Muller-Eberhard U, Morgan WT. Porphyrin-binding proteins in serum. Ann NY Acad Sci 1975;244:624-650.
37. Adams PA, Berman MC. Kinetics and mechanism of the interaction between human serum albumin and monomeric haemin. Biochem J 1980;191:95-102.
38. Wardell M, Wang Z, Ho JX, Robert J, Ruker F, Rubel J, Carter DC. The atomic structure of human serum methemalbumin at 1.9 Å. Biochem Biophys Res Commun 2002;291:813-819.
39. Zunszain PA, Ghuman J, Komatsu T, Tsuchida E, Curry S. Crystal structural analysis of human serum albumin complexed with hemin and fatty acid. BMC Struct Biol 2003;3:6.
40. Komatsu T, Ohmichi N, Nakagawa A, Zunszain PA, Curry S, Tsuchida E. O_2 and CO binding properties of artificial hemoproteins formed by complexing iron protoporphyrin IX with human serum albumin mutants. J Am Chem Soc 2005;127:15933-15942.
41. Phillips SEV, Schoenborn BP. Neuteon diffraction reveals oxygen-histidine hydrogen bond in oxymyoglobin. Nature 1981;292:81-82.
42. Shaanan B. Structure of human oxyhemoglobin at 2.1 Å resolution. J Mol Biol 1983;171:31-59.
43. Komatsu T, Nakagawa A, Zunszain PA, Curry S, Tsuchida E. Genetic engineering of the heme pocket in human serum albumin: modulation of O_2 binding of iron protoporphyrin IX by variation of distal amino acids. J Am Chem Soc 2007;129:11286-11295.
44. Kalyanasundaram K, Grätzel M. Light induced redox reactions of water soluble porphyrins, sensitization of hydrogen generation from water by zincporphyrin derivatives. Helv Chim Acta 1980;63:478-485.
45. Komatsu T, Wang RM, Zunszain PA, Curry S, Tsuchida E. Photosensitized reduction of water to hydrogen using human serum albumin complexed with zinc-protoporphyrin IX. J Am Chem Soc 2006;128:16297-16301.
46. Dougherty TJ. Studies on the structure of porphyrins contained in Photofrin-II. Photochem Photobiol 1987;46:569-573.
47. Dougherty TJ, Gomer CJ, Henderson BW, Jori G, Kessel D, Korbelik M, Moan J, Peng Q. Photodynamic therapy. J Natl Cancer Inst 1998;90:889-905.
48. Lopez RFV, Lange N, Guy R, Bentley MVLB. Photodynamic therapy of skin cancer: controlled drug delivery of 5-ALA and its esters. Drug Deliver Rev 2004;56:77-94.
49. Aveline B, Hasen T, Redmond RW. Photophysical and photosensitizing properties of benzoporphyrin derivative monoacid ring A (BPD-MA). Photochem Photobiol 1994;59:328-335.
50. Guldi DM, Prato M. Excited-state properties of C_{60} fullerene derivatives. Acc Chem Res 2000;33:695-703.
51. Arbogast JW, Darmanyan AP, Foote CS, Rubin Y, Diederich FN, Alvarez MM, Anz SJ, Whetten RL. Photophysical properties of C_{60}. J Phys Chem 1991;95:11-12.
52. Anderson JL, An YZ, Rubin Y, Foote CS. Photophysical characterization and single oxygen yield of a dihydrofullerene. J Am Chem Soc 1994;116:9763-9764.
53. Qu X, Komatsu T, Sato T, Glatter O, Horinouchi H, Kobayashi K, Tsuchida E. Structure, photophysical property, and cytotoxicity of human serum albumin complexed with tris (dicarboxymethylene)[60]fullerene. Bioconjugate Chem 2008;19:1556-1560.
54. Wilkinson F, Helman WP, Rossa AB. Quantum yields for the photosensitized formation of the lowest electronically excited singlet-state of molecular-oxygen in solution, J Phys Chem Ref Data 1993;22:113-262.
55. Lu G, Komatsu T, Tsuchida E. Artificial hemoprotein nanotubes. Chem Commun 2007;2980-2982.
56. Lu G, Tsuchida E, Komatsu T. Human serum albumin nanotubes comprising layer-by-layer assembly with polycation. Chem Lett 2008;37:972-973.
57. Qu X, Lu G, Tsuchida E, Komatsu T. Protein nanotubes comprised of an alternate layer-by-layer assembly using a polycation as an electrostatic glue. Chem Eur J 2008;14:10303-10308.

Microvascular Reviews and Communications

Vol.3 No.1

Exogenous nitric oxide increases microflow but decreases RBC attendance in single capillaries in rat cerebral cortex

Minoru Tomita[1)], Takashi Osada[1)], Miyuki Unekawa[1)], Yutaka Tomita[1)], Haruki Toriumi[1)] and Norihiro Suzuki[1),*]

1) Department of Neurology, School of Medicine, Keio University

Abstract

The effects of nitric oxide (NO) on microflow and capillary red blood cell (RBC) velocity of the cerebral cortex were examined in 5 urethane-anesthetized rats through an open cranial window. Changes in microflow were evaluated with hemodilution technique with in-house Matlab-domain software, KEIO-IS1, presented as a 2-D microflow-map. When FITC-labeled RBCs were injected into the femoral vein, they appeared in the microvasculature of the cerebral cortex including capillaries. Changes in RBC velocity and attendance in single capillaries were determined with a high-speed camera laser scanning confocal fluorescence microscope before, during and after NO administration. The velocity and number of RBCs in the ROI were calculated with KEIO-IS2. Nitroprusside (a NO donor) was administered topically on the exposed brain surface, additionally microinjected into the tissues in 3 rats, and further intravenously in 2 rats. We found that: 1) NO increased microflow markedly regardless of the routes of administration and when limited to the cases of topical application microflow increased by 182±22 % (mean ± SD) of control ($P<0.01$). 2) RBC velocity in capillaries remained broadly unchanged, whereas RBC number (attendance) decreased in all cases ($P<0.05$). We interpreted that NO induced an increase in microflow not through nutritional capillaries but via other pathways from artery to veins, *e.g.*, thoroughfare channels. This finding suggests the presence of an independent velocity-impedance mechanism at the level of individual single capillaries in which excessive increase in capillary flow is somehow prevented. [MVRC 3(1): 11-16, 2009]

Key words: capillary flow, flow regulation, neuro-capillary coupling, RBC velocity, single capillary, tissue perfusion

Received 2009/4/4, Accepted 2009/8/4

*To whom correspondence should be addressed: Norihiro Suzuki, MD. PhD. Department of Neurology, School of Medicine, Keio University
35 Shinanomachi, Shinjuku-ku, Tokyo 160-8582, Japan
TEL: 81-3-3353-1211 FAX: 81-3-3353-1272
E-mail: nrsuzuki@sc.itc.keio.ac.jp

Introduction

Arterioles have been implicated in the control of capillary flow, feeding nutrition to neurons which dispatch time-to-time feedback signals to the arterioles concerning their nutritional requirements arising from their functional activities. However, recent studies have revealed that sudden neuronal activation causes capillary flow changes on a time scale of less than 1 s[1]. This time seems to be too short for the response to be controlled by arterial blood supply, suggesting the existence of a direct flow control mechanism operating from neurons to nearby capillaries. We showed RBC capillary flow decrease when cortical spreading depression and therefore neuronal depolarization was induced by potassium application on the brain surface of rats[2]. Involvement of intrinsic nitric oxide (NO) as a chemical mediator from neurons to capillary was postulated by Hudetz[3]. In fact, it is a gaseous material, which would afford a very rapid response in vascular dilatation[4] or tonic regulation[5]. However, capillary does not have muscles in possession. NO has a dual effect on cerebral tissue: NO is a poison that rapidly intoxicates neurons[6,7], while it increases cerebral blood flow greatly. It is still unclear whether or not exogenous NO is beneficial to neurons under ischemic conditions.

The aim of this study is to investigate the effects of exogenous nitric oxide (NO) on RBC velocity changes in cortical single capillaries following application of NO via various routes.

Methods and Materials

Five Wistar male rats were used. The experiments were approved by the Animal Ethics Committee of Keio University, and experimental procedures were performed in accordance with the University guidelines for the care and use of laboratory animals. The effects of nitric oxide (NO) on microflow whose definition will be given below and red blood cell (RBC) velocity in single capillaries were examined in urethane-anesthetized rats through an open cranial window. A femoral artery and a femoral vein were catheterized to measure blood pressure (SABP) and to allow administration of FITC-labeled RBC suspension prepared beforehand, respectively. A catheter was also inserted into the internal carotid artery for the injection of a small amount of saline (we used the saline as a negative indicator of blood in the present study). The external carotid artery was tied to avoid indicator escaping to the external carotid system. The animals were placed on a head holder with ear bars. A 5-mm-diameter cranial window was trephined above the left temporoparietal cortex and the dura was removed. The microvasculature in the cortical tissue was continuously videotaped with a conventional 30 fps (frames per second) video camera (Fig. 1). A FITC-labeled RBC suspension was injected into the femoral vein so that the labeled RBCs were circulating at the concentration of 0.4% of the total RBCs for approximately 3 hours after the injection.

Microflow: The principle and assumptions underlying the measurements of flow in 'pixels' (100 averaged Scion pixels or practical size 40 μm × 40 μm) were described elsewhere[8]. Briefly, when a dye was injected into the internal carotid artery, the dye was distributed to microvasculature to all corners of cerebral cortex: the bolus of blood passed through all pixels producing time-variable concentration

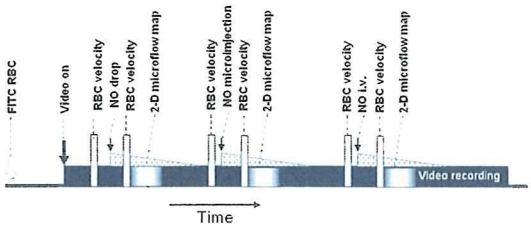

Fig. 1. Protocol of experimental procedure. Video recording of brain surface started at the closed arrow. NO was applied on the brain surface at NO drop. RBC velocity and number was measured with the high-speed camera laser scanning confocal fluorescence microscope during 10 s at the empty square. At the whitening marks in the dark bar, small amount of saline was injected into the internal carotid artery to produce hemodilution process which was recorded on the video tape and analyzed with KEIO-IS1. The dotted triangle area indicates NO effective period. NO was microinjected into the cortex and above set measurements were repeated. At NO i.v., NO was injected intravenously into the circulating blood. Above set measurements were repeated.

changes in the pixel as appearance, peaking and disappearance reflecting blood flow rapidity. The cortical images with dye dilution process were continuously recorded on videotape at 30 fps or directly fed into a personal computer through a Scion LG-3 frame grabber card (Scion Corporation, MD, USA). The dye dilution curves for all the individual pixels of an approximately more than 50 × 50 matrix (the size of the matrix was automatically decided by the computer in the ROI of ca. 4 mm × 5 mm) were all together analyzed with in-house Matlab-domain software, KEIO-IS1*1 to evaluate the MTTs by employing a customized algorithm of the area/height of hemodilution curves ($MTT = \int t.c(t)dt / \int c(t)dt$ where c is the optical density change in a pixel). The reciprocal mean transit time (1/MTT) was taken to represent the microflow (so termed by us), which was arranged in appropriate coordinates to construct a two-dimensional (2-D) microflow map with aid of KEIO-IS1. The 2-D flow map had a resolution of 625 flow values/mm^2, which is ca. 500-fold higher spatial resolution than that of conventional laser Doppler flowmetry. The KEIO-IS1 thus calculated automatically all pixular flow values in the region of interest (ROI) yielding a distribution curve of individual miroflows, and displayed a 2-D microflow map together with the histograms of microflow plotted against magnitude of flow rates. The unit of microflow was just relative or flow index relative to the control. However, time to time and location to location changes in flow value could be quantitatively compared.

---

*1 KEIO-IS1 (Patent No. 4068098) has potentially a wide applicability to analyze videotaped optical density changes of dye-dilution process in various organs, e.g., heart, liver, skin, stomach etc., to calculate reciprocal mean transit times of a dye, microflow mapping and analysis of microcirculatory parameters such as mean of flow values, standard deviation, skewness and kurtosis employing the moment analysis formula9). IS stands for initials of Istvan Schiszler, a Hungarian MD who stayed with us at age 26 (1998-2001) as a JSPS researcher. KEIO-IS2 (Patent No 4068099) has also been developed by him with a wide applicability to trace or track movements of fluorescence labeled cells or molecules. Those who are interested in the softwares running on PC, please contact Yutaka Tomita <yutakacnrs@aol.com>.

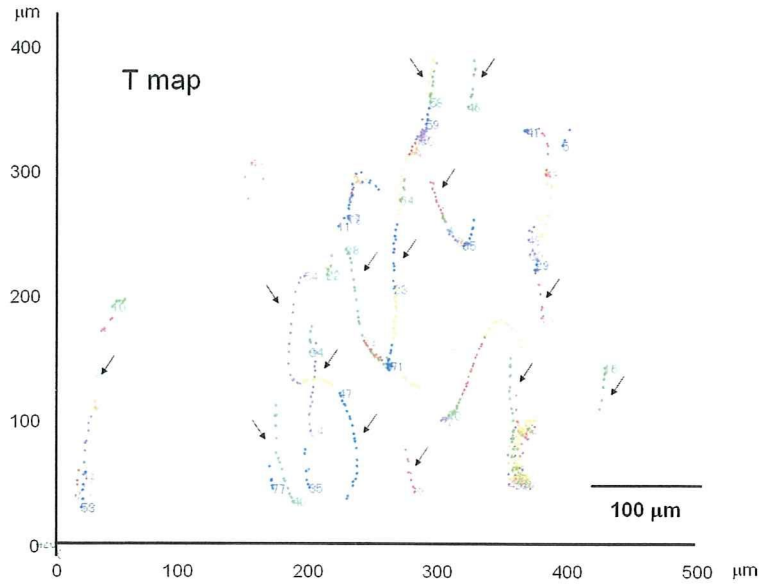

Fig. 2. RBC tracking map (T map) obtained with KEIO-IS2 from a 2 s video clip taken at 500 fps. Frame-by-frame movements of all RBCs appearing in the sequential 1000 frames are all shown. RBCs were automatically numbered in order of appearance. Arrows indicate RBC tracking in single capillaries.

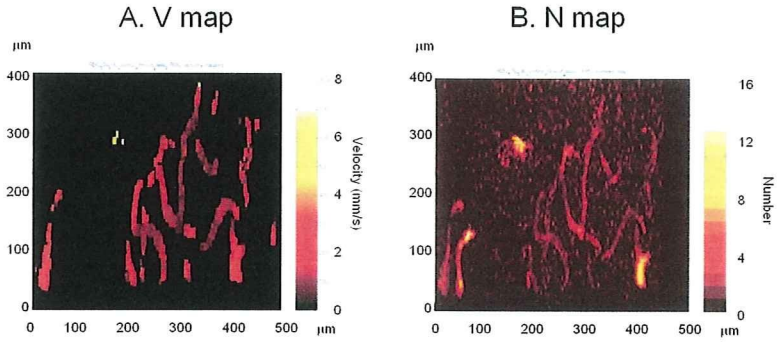

Fig. 3. A. RBC velocity map (V map) and B. RBC number map (N map), calculated with KEIO-IS2 from the same video clip as used for Figure 2. Color scales are shown at the right of the each figure. The RBC velocities in V map were calculated from moved distances per frame multiplying by the frame rate (500 fps). N map represents all RBCs that appeared in the ROI during 2 s, or integration of all 1000 frames. Note that the V map and N map resemble each other although their image elements were different.

Capillary RBC velocity: RBC velocity in single capillaries was examined with microscope in a central small area of 400 μm × 500 μm in the same cortical area as used for the above microflow measurement (the area was approximately 1/100th of a 2-D microflow map). The measurement was done by switching the optical system to a high-speed camera laser scanning confocal fluorescence microscope. A tracer FITC-labeled RBC which had been injected previously into the femoral vein was seen in arteries, capillaries and veins in the cortical microvasculature. The vast number of RBCs were analyzed with in-house Matlab-domain software, KEIO-IS2[10,11]. The software KEIO-IS2 automatically calculated velocities of all RBCs and displayed an RBC tracking map (T map, Fig. 2), an RBC velocity map (V map, Fig. 3: left), and an RBC number map (N map, Fig. 3: right). The numerical data of individual RBC velocities in single capillaries were further exported to a Microsoft Excel spreadsheet for statistical analyses[12]. On the tracking map, we sorted RBCs flowing in single capillaries (Fig. 2) and their velocities and numbers were exported to a spreadsheet Excel for further statistical analysis.

NO administration: A small amount of nitroprusside (3-5 mg/ml), a donor of NO, was topically applied in all cases on the brain surface. Additional application was made intraparenchymally with a microinjector in 3 cases, and intravenously from the femoral vein (i.v.) in 2 cases. The experimental protocols were schematically summarized in Figure 1. FITC-labeled RBC was injected into the femoral vein (at the empty arrow). Video recording made throughout the experiments starting at the closed arrow. NO was applied on the brain surface at mark A. Recording with high-speed camera laser scanning confocal fluorescence microscope during 10 s was interspaced at empty squares to monitor RBC movements for the calculation of RBC velocity and

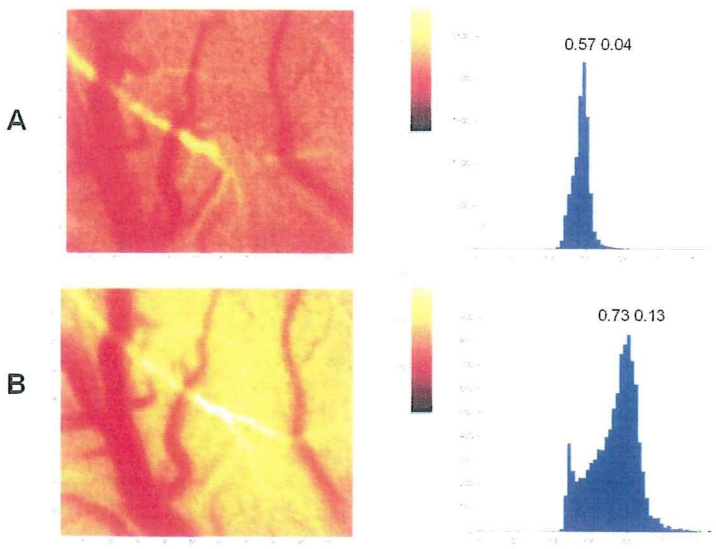

Fig. 4. A. 2-D microflow map (left) and histogram of microflow (right) in control state. A high flow arteriole (yellow) is seen running from left top to the center, and three veins running from top to bottom in red. B. Microflow increases in the center where NO was dropped. An increase in high flow component is seen in the histogram.

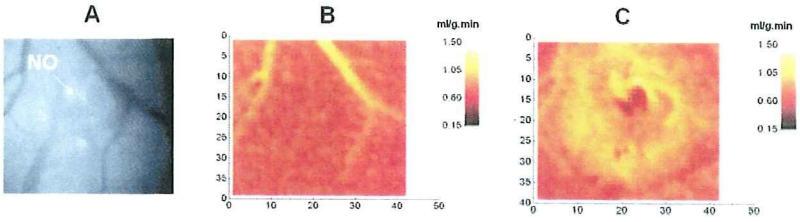

Fig. 5. A. A microphotograph of the exposed cerebral cortex. At arrow NO was microinjected. B. Two-dimensional microflow map of A. The microphotograph and the 2-D microflow map look similar although the two images were composed of different image elements demonstrating the validity of the technique. C. Wave-ring spread of microflow increase expanding coaxially with time.

number. Saline injection into the internal carotid artery was made at the graded white mark in the dark bar to produce hemodilution in the observing tissue area. Predicted period of NO effect was shown in the dotted triangle area. NO was then microinjected into the cortex at B and the same set measurement procedure was repeated. Finally, NO was slowly injected intravenously into the circulating blood at C. Above set measurement procedure was repeated.

In all experiments, SABP was routinely recorded via a strain gage transducer connected to the femoral arterial catheter on a personal computer (PC) with Acknowledge software (MP 100 WS).

Results

Microflow increase with NO: Figure 4 shows a typical example of 2-D microflow map (A, left) and microflow histogram (A, right) in control state, and those (B, left and right) after topical application of NO on the cortical surface. There is a yellow color artery, red color veins and capillaries with the color scale for the flow rate. Microflow increased almost 2 fold in the location where NO was dropped and spread. The mode of the increase of microflow is shown in the right hand component of the histogram. Calculated average flow (the mean of the histogram) was increased with NO from 0.57 to 0.73, and the maximum increase was from 0.63 to 2.22 at the center of the yellow area. When NO was microinjected into the cortical tissue shown in a microphotograph (Fig. 5A), a wave-ring spread of increasing microflow took place coaxially to the injection site as shown in Figure 5C. The mode of wave-ring spread was quite similar to that seen during cortical spreading depression induced by local microinjection of potassium into the rat cerebral cortex[13,14]. Figure 5A (microphotograph) and Figure 5B (2-D microflow map) appeared to be quite similar, but picture elements were different: the former consisted of optical brightness and the latter flow components (1/MTT). Figure 6 shows 2-D microflow maps of different routes of NO application: drop application (B), and i.v. application (C). Note that a tremendous increase in microflow when NO was applied topically. SABP was decrease by 20 % each time even when a small amount of NO was applied topically. The NO must be taken up from the brain tissue by the circulating blood and the trace amount of NO in the circulating blood dilated systemic arteries causing blood pressure drop. The microflow increase after i.v. NO administration was

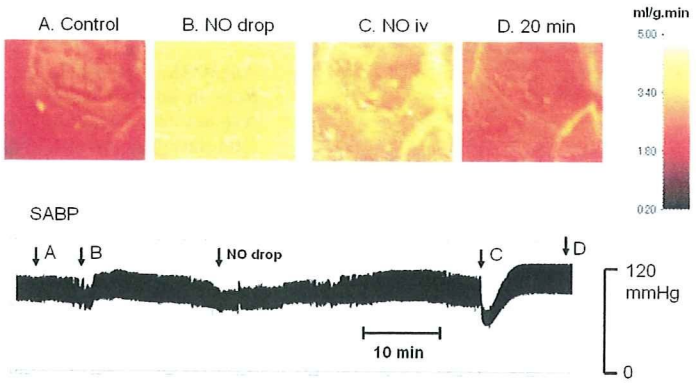

Fig. 6. Top: Sequentially arranged 2-D flow maps to show a marked increase in microflow (B) following topical application of NO on the brain surface, and a less increase in microflow following NO i.v. infusion. Bottom: Continuous recording of SABP. Topical application of NO decreased SABP by 20 %. NO i.v. administration elicited a rapid fall in SABP.

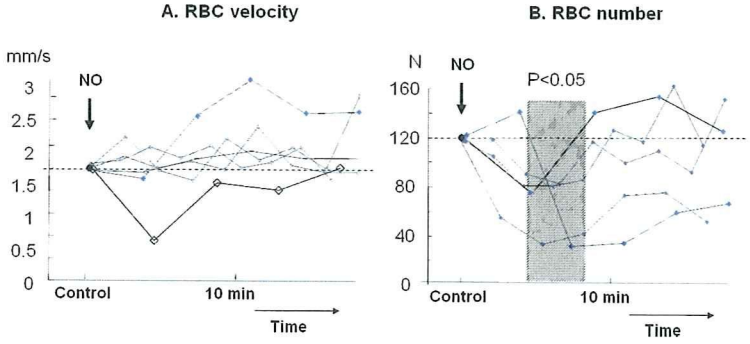

Fig. 7. A. Time courses of RBC velocity changes in single capillaries after NO administration, showing no apparent change in RBC velocity as an average. B. RBC number in single capillaries decreased in all 5 cases ($P<0.05$) in the shaded area, with a subsequent gradual recovery.

less than that of topical application. This could be due to a marked SABP fall as shown at C.

When collected microflow values induced by NO topical application at the center in all 5 cases were from 0.97±0.24 to 1.89±0.36 (Table 1), approximately doubled (182±22 % of the control), whose change was statistically significant ($P<0.01$, student paired t-test).

Capillary RBC velocity changes with NO: In contrast to rather uniform increase in microflow, responses of RBC velocity in single capillaries were variable: an increase, unchanged and decrease (Fig. 7. A). Such variable responses were observed even in an intraindividual case: the first response was a marked increase in velocity while the second rather decreasing. As shown in Figure 7A. RBC velocity appeared to be unchanged when averaged for all 5 cases. RBC number, on the other hand, decreased in all cases ($P<0.05$, student nonparametric t-test against null hypothesis) as shown by the samples in the shaded area in Figure 7B, which were followed by a tendency of recovery. In 2 cases, moving RBCs were voided from intraparenchymal single capillaries in the ROI. The RBC disappearance lasted for a couple of minutes, and RBCs reappeared to the previous level thereafter. We speculate that voiding of RBCs from single capillaries may be due to a capillary response to transient neuronal dysfunction resulting from NO toxicity, even though NO dilated arterioles to increase microflow, presumably through blood-shunting channels (so-called thoroughfare channels). In general, the comparison was difficult because capillaries in the ROI changed with NO administration due probably to tissue volume change by NO. In most of cases refocusing was required after the NO effect.

Table 1. Microflow change

	Control	NO
	0.63	2.22
	0.91	1.58
	0.95	1.61
	1.05	1.72
	1.3	2.35
Mean	0.96	1.89
SD	0.24	0.36

$P<0.01$

Summary of the present experiments was shown in Figure 8. NO increased microflow greatly whereas corresponding capillary RBC flow (velocity × number) remained unchanged or even decreasing.

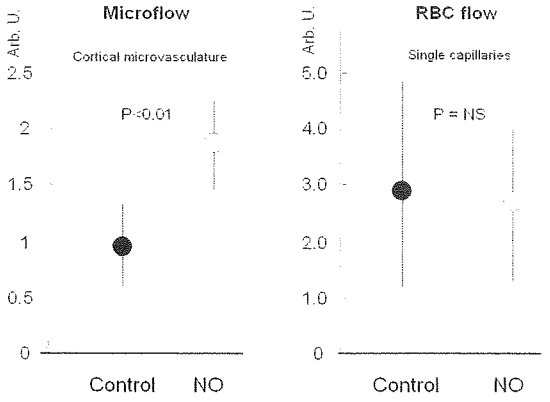

Fig. 8. To show a contrast of the marked increase in microflow upon NO topical application (left), and an unchanged RBC flow (right) as calculated from RBC velocity change multiplied RBC number change in the single capillaries of the tissue. Both discrepant changes occurred simultaneously in the same cortical tissue microvasculature.

Discussion

It is well known that NO dilates cerebral arteries and increases cerebral blood flow. This was shown in the present experiments as NO increased microflow greatly. However, unexpectedly, RBC flow in capillaries was not compliant to the arterial flow. RBC velocity change was unchanged as an average of diverse responses, but RBC number decreased in the capillaries. Since RBC is oxygen carrier, RBC decrease in capillaries may result in hypoxia in the tissue. It is paradoxical that microflow increases almost doubled whereas the tissue becomes hypoxic, which is, however, just predicted, and has not been proved yet. Further speculation is that arteriolar regulation governs total tissue perfusion including microflow and thoroughfare channels, but not individual capillaries which would somehow be protected from unnecessary flow increase in certain circumstances. Two possibilities which explain plausibly the capillary flow dissociation from the arterial flow increase are that 1) neurons would cause RBC voiding from nearby capillaries, or 2) capillary lumen would be narrowed by thickening of peripheral layer of plasma with increasing viscosity or by pericyte constriction. Hudetz *et al.*[3], and Hudetz[4] considered that neuronal intrinsic NO may be the mediator to control capillary flow, but our observation does not support his hypothesis. It is not conclusive since we used exogenous NO, and the excessive amount might induce an untoward effect to neurons.

In our observations, two points may be of clinical relevance. The first is that NO (either Nitrol or NO skin patch for coronary spasm) often develops headache, flush face and light headedness. The latter symptom may be explained by the transient tissue hypoxia. The second is that NO is often used to decrease high blood pressure especially during surgical operation on the brain. Our experiment showed that overdose of i.v. NO developed severe hypotension and brain swelling with tissue hypoxia.

References

1) Ances BM., Greenberg JH. and Detre JA.: Effects of variations in interstimulus interval on activation-flow coupling response and somatosensory evoked potentials with forepaw stimulation in the rat. *J. Cereb. Blood Flow Metab.*, **20**: 290-297, 2000.
2) Tomita M., Tomita Y., Toriumi H., Unekawa M. and Suzuki N.: Coupling of capillary RBC flow failure with neuronal depolarization. *Available from Nature Precedings*. 2009. http://precedings.nature.com/documents/3220/version/1
3) Hudetz AG.: Blood flow in the cerebral capillary network: a review emphasizing observations with intravital microscopy. *Microcirculation*, **4**: 233-252, 1997.
4) Hudetz AG., Shen H. and Kampine JP.: Nitric oxide from neuronal NOS plays critical role in cerebral capillary flow response to hypoxia. *Am. J. Physiol.*, **274**: H982-989, 1998.
5) Ishikawa M., Kajimura M., Adachi T., Maruyama K., Makino N., Goda N., Yamaguchi T., Sekizuka E. and Suematsu M.: Carbon monoxide from heme oxygenase-2 is a tonic regulator against NO-dependent vasodilatation in the adult rat cerebral microcirculation. *Circ. Res.*, **97**: E104-114, 2005.
6) Okuma Y., Uehara T. and Nomura Y.: The precise characterization and the crucial mechanism of NO-induced cytotoxicity (Review in Japanese). *Nippon Yakurigaku Zasshi*, **112**: 187-194, 1998.
7) Yanamoto K., Hosoi R., Uesaka Y., Abe K., Tsukada H. and Inoue O.: Intrastriatal microinjection of sodium nitroprusside induces cell death and reduces binding of dopaminergic receptors. *Synapse*, **50**: 137-143, 2003.
8) Schiszler I., Tomita M., Fukuuchi Y., Tanahashi N. and Inoue K.: New optical method for analyzing cortical blood flow heterogeneity in small animals: validation of the method. *Am. J. Physiol.*, **279**: H1291-1298, 2000.
9) Tomita M., Gotoh F., Amano T., Tanahashi N., Kobari M., Shinohara T. and Mihara B.: Transfer function through regional cerebral cortex evaluated by a photoelectric method. *Am. J. Physiol.*, **245**: H385-H398, 1983.
10) Schiszler I., Takeda H., Tomita M., Tomita Y., Osada T., Unekawa M., Tanahashi N. and Suzuki N.: Software (KEIO-IS2) for automatically tracking red blood cells (RBCs) with calculation of individual RBC velocities in single capillaries of rat brain (abstr.). *J. Cereb. Blood Flow Metabol.*, **25**: S541, 2005.
11) Tomita M., Osada T., Schiszler I., Tomita Y., Unekawa M., Toriumi H., Tanahashi N. and Suzuki N.: Automated method for tracking vast numbers of FITC-labeled RBCs in microvessels of rat brain in vivo using a high-speed confocal microscope system. *Microcirculation*, **15**(2): 163-174, 2008.
12) Unekawa M., Tomita M., Osada T., Tomita Y., Toriumi H., Tatarishvili J. and Suzuki N.: Frequency distribution function of RBC velocities in single capillaries of the rat cerebral cortex using intravital confocal microscope with high-speed camera. *Asian Biomed.*, **2**(3): 203-218, 2008.
13) Tomita Y., Tomita M., Schiszler I., Amano T., Tanahashi N., Kobari M., Takeda H. and Ohtomo M.: Repetitive concentric wave-ring spread of oligemia/hyperemia in the sensorimotor cortex accompanying K^+-induced spreading depression in rats and cats. *Neurosci. Lett.*, **322**: 157-160, 2002.
14) Tomita M., Schiszler I., Tomita Y., Tanahashi N., Takeda H., Osada T. and Suzuki N.: Initial oligemia with capillary flow stop followed by hyperemia during K^+-induced cortical spreading depression in rats. *J. Cereb. Blood Flow Metab.*, **25**: 742-747, 2005.

Stroke

JOURNAL OF THE AMERICAN HEART ASSOCIATION

American Stroke Association

A Division of American Heart Association

Dually Supplied T-Junctions in Arteriolo-Arteriolar Anastomosis in Mice: Key to Local Hemodynamic Homeostasis in Normal and Ischemic States?

Haruki Toriumi, Jemal Tatarishvili, Minoru Tomita, Yutaka Tomita, Miyuki Unekawa and Norihiro Suzuki

Stroke 2009;40;3378-3383; originally published online Aug 6, 2009;
DOI: 10.1161/STROKEAHA.109.558577
Stroke is published by the American Heart Association. 7272 Greenville Avenue, Dallas, TX 72514
 Print ISSN: 0039-2499. Online ISSN: 1524-4628

Dually Supplied T-Junctions in Arteriolo-Arteriolar Anastomosis in Mice

Key to Local Hemodynamic Homeostasis in Normal and Ischemic States?

Haruki Toriumi, M.Med.Sci.; Jemal Tatarishvili, MD, PhD; Minoru Tomita, MD, PhD; Yutaka Tomita, MD, PhD; Miyuki Unekawa, PhD; Norihiro Suzuki, MD, PhD

Background and Purpose—The functional role of arteriolo-arteriolar anastomosis (AAA) between the middle cerebral artery (MCA) and anterior cerebral artery in local hemodynamics is unknown, and was investigated here.

Methods—Blood flow in AAAs was examined using fluorescein isothiocyanate–labeled red blood cells (RBCs) as a flow indicator in 16 anesthetized C57BL/6J mice before and after MCA occlusion up to 7 experimental days.

Results—We observed paradoxical flow in AAAs; labeled RBCs entered from both the MCA and anterior cerebral artery sides and the opposing flows met at a branching T-junction, where the flows combined and passed into a penetrating arteriole. The dually fed T-junction was not fixed in position, but functionally jumped to adjacent T-junctions in response to changing hemodynamic conditions. On MCA occlusion, RBC flow from the MCA side immediately stopped. After a period of "hesitation," blood started to move retrogradely in one of the MCA branches toward the MCA stem. The retrograde blood flow was statistically significantly ($P<0.05$), serving to feed blood to other MCA branches after a lag period. In capillaries, MCA occlusion induced immediate RBC disappearance in the ischemic core and to a lesser extent in the marginal zone near AAAs. At day 3 after ischemia, we recognized the beginning of remodeling with angiogenesis centering on AAAs.

Conclusions—AAAs appear to play a key role in local hemodynamic homeostasis, both in the normal state and in the development of collateral channels and revascularization during ischemia. (*Stroke*. 2009;40:3378-3383.)

Key Words: arterio-arterial anastomosis ■ angiogenesis ■ cerebral ischemia ■ penumbra ■ red blood cell

Michedlishvili[1] reported abundant arteriolo-arteriolar anastomoses (AAAs) connecting cerebral arterioles, based on his extensive microscopic study of cerebral microcirculation in the brains of many animals, including hens, rabbits, cats, dogs, and monkeys. By filling vessels with carbon black-labeled latex (Vultex), Coyle and Jokelainen[2] investigated the vascular structure of major cerebral arteries in detail and found that there were about 29 anterior cerebral artery (ACA)/middle cerebral artery (MCA) junctions per hemisphere in normal Wistar rats. The supplying territories of the major cerebral arteries were interconnected by functional anastomoses forming boundary zones between the superficial pial arteries, constituting the so-called cortical watershed.[3,4] However, little is known about the hemodynamic characteristics of AAAs involved in peripheral collateral pathways under normal and ischemic conditions. An unanswered question is whether or not flow exists in AAAs caught between 2 opposing arterial pressures, and if it does, what is the direction of flow in the connecting arterioles. Ganushkina et al[5] reported that there was no flow, and that there was only plasma at the dead point of blood in AAAs. However, if no flow occurred in the channel, RBC aggregation would occur and the vessel would eventually become closed. Clinically, the issue seems relevant to hemodynamic compensation in watershed areas during ischemia and the development of collateral channels. If flow rescue fails, watershed infarction might theoretically ensue.

The main goal of this study was to investigate the functional role of AAA between MCA and ACA in mice before and after ischemia, by visualization of flow with fluorescein isothiocyanate (FITC)-labeled red blood cells (RBCs)[6] and a high-speed camera laser scanning confocal fluorescence microscope system recently developed by us.[7] We used a mouse model developed by Seylaz et al.[8]

Materials and Methods

Sixteen male C57BL/6J mice (10 weeks old) weighing 20 to 25 g, purchased from Animal Supply (Nihon Kurea International, Tokyo, Japan), were used under isoflurane (1.4 to 1.8%) aesthesia. Eight mice were used for 1-day experiments (acute), 8 mice for 2- to 7-day experiments (chronic), and 2 after acute experiments for Mercox

Received May 25, 2009; accepted June 16, 2009.

From the Departments of Neurology (H.T., J.T., M.T., Y.T., M.U., N.S.) and Preventive Medicine for Cerebrovascular Disease (Y.T.), School of Medicine, Keio University, Tokyo Japan.

H.T. and J.T. contributed equally to this article.

Correspondence to Minoru Tomita, MD, PhD, 35 Shinanomachi, Shinjuku-ku, Tokyo 160-8582, Japan. E-mail mtomita@sc.itc.keio.ac.jp

Stroke is available at http://stroke.ahajournals.org DOI: 10.1161/STROKEAHA.109.558577

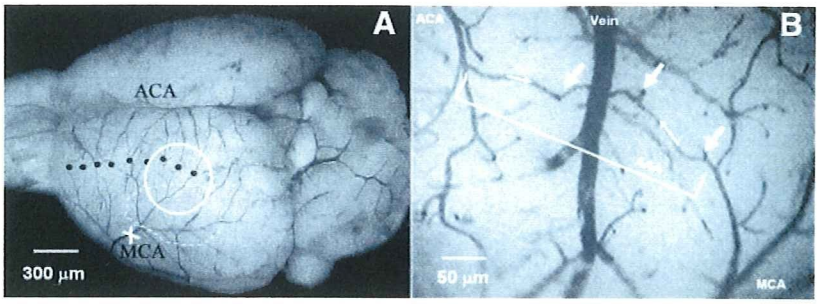

Figure 1. A, Dorsal view of epicortical arteries on the removed mouse brain after intravascular injection of Mercox containing carbon black. Black dots indicate arteriolo-arteriolar anastomoses (AAA) between the anterior cerebral artery (ACA) and middle cerebral artery (MCA). The white cross indicates the site of MCA occlusion. The white circle is the position of the cranial window and the dotted line circle denotes the approximate location of the ischemic core. B, An AAA of living brain indicated by a white line, with a large cortical vein crossing in the center. In the AAA, there are 3 T-junctions indicated by arrows. Small arrows indicate the directions of opposing blood flow (see text for further explanation).

filling experiments. All experimental procedures were performed in accordance with the University's guidelines for the care and use of laboratory animals, with the approval of the Animal Ethics Committee of Keio University. Preliminary surgical procedures were performed by using a surgical microscope (OPMI Pico, Carl Zeiss) as described by Tomita.[8] Briefly, a 3-mm diameter hole was drilled above the left parieto-temporal cortex, 1 mm lateral from the sagittal suture and 1 mm posterior from the bregma. To avoid drying of the tissue and to keep the brain surface sterile for the chronic experiment, the trepanation was covered with a circular 140-μm thick quartz glass window, sealed onto the bone with dental cement (Ionosit, DMG). The area under the window corresponded to a supplying territory of distal branches of both the MCA and ACA. In 2 mice under deep anesthesia which were used for acute experiments, Mercox mixed with carbon black was injected into the heart to fill the cerebral microvasculature, including AAAs. After removal of the whole brain, the microvasculature on the brain surface was viewed and photographed from above to examine arteriolar connections between MCA and MCA (Figure 1A).

To visualize blood flow changes in an AAA, we traced FITC-labeled RBCs and measured RBC velocities in the connecting branches of MCA and ACA before and after MCA occlusion (MCAO). A suspension of mouse RBCs labeled beforehand with FITC[7] was injected into the systemic circulation through the tail vein. The mouse head was fixed to a special head holder with a metal bar securely cemented at the posterior edge of the skull bone. The bar was used to finely adjust the ROI in the brain surface stereotaxically to the same position in x-y-z coordinates so that the same site could be visualized consistently. A high-speed camera laser scanning confocal fluorescence microscope system recently developed by us was used for RBC velocity measurements.[6] The microscope was equipped with a objective lens (Nikon LU Plan EPI SLWD 4×, 10×, and 20×) and a halogen lamp for obtaining a general view of the brain microcirculation with a video camera (30 fps, DCR-PC100, Sony); output was recorded on-line. Laser illumination (λ= 488 nm; Melles Griot) was used for observation of tracking and velocities of FITC-labeled RBCs with a high-speed camera (500 fps) in an optical slice of ≈20 μm in thickness. Evaluation of the RBC tracking and velocities in single microvessels was performed by using the Matlab domain KEIO-IS2 software.[6] Wall shear rates (gw) of blood flow in AAA were calculated from the RBC velocities thus obtained by application of the following equation

$$\gamma w = 4v/r = 4Q/\pi r^3 \quad (1)$$

where v is the velocity, r the radius (half of the diameter) of AAA, and Q the blood flow.[9]

After control observations of RBC flow the mouse was subjected to cerebral ischemia by occluding the proximal branch of the MCA (Figure 1A), using a slight modification of Tamura's original method.[10] Capillary network changes were examined with rhodamine isothiocyanate (RITC) dextran (λ=533 nm), which was injected into the tail vein and subsequently filled the capillaries in tissues, including the cerebral cortex.

In chronic experiments in 8 mice, after the observation of AAA and related microvasculature through the cranial window, which took approximately 1 hour, the mouse was returned to the animal center. Next day, the mouse was brought back to the laboratory and fixed in the holder, which was adjusted so that the same AAA and microvasculature as before could be observed, and FITC-labeled RBCs were injected into the tail vein. This procedure was repeated every day for a week. The AAA and microvascular changes were evaluated from the videotape recordings. Vascular structural changes were examined by the use of RITC dextran when required.

Results

Arteriolo-Arteriolar Anastomosis Before MCAO (Normal or Control Condition)

Three-Dimensional Structural Characteristics

Figure 1A is a dorsal overview of the epicortical pial arterial network filled with carbon black mixed in Mercox. Only cerebral arteries and arterioles were visualized, apparently because Mercox has such a high viscosity that it could not fill the veins. Dark dots in Figure 1A indicate the connecting points in the watershed area between peripheral branches of the MCA and ACA, representing arteriolo-arteriolar anastomoses (AAA). Figure 1B shows an enlarged microphotograph of an AAA in situ, running across the ROI under a large vein in the cerebral cortex. As indicated by arrows, there were 3 T-junctions of penetrating arterioles (this will be discussed later). The mean diameter of such connecting distal branches of MCA and ACA was 27±2.5 μm (mean±SD, n=8). However, the diameter of AAAs tended to be different depending on location along the channel: the average diameter was larger in the center of an anastomosis (28±2.5 μm, n=8) than at proximal sites (20±1.9 μm, n=8).

Direction of Flow in AAA

During continuous recorded observation of the cortical microvascular image of the watershed area with the fluorescence microscope through the skull window, a suspension of FITC-labeled RBCs was injected into the circulating blood through the tail vein so that its final concentration in the circulating blood became 0.4% of total RBCs. The labeled RBCs appeared in the capillary network of the microvasculature in the cortex like fireflies on a dark background. Interestingly, when the labeled RBCs arrived at an AAA, they

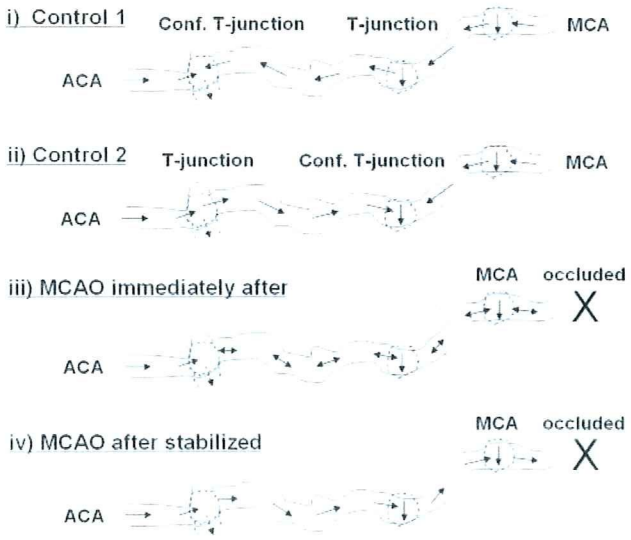

Figure 2. Changes in flow direction in an AAA under various conditions, as detected by tracing FITC-labeled RBCs. Conf. T-junction means that opposing blood flows passed together confluently into the same penetrating arteriole (see text for further explanation).

progressed into it from both the ACA and MCA sides (Figure 1B). The 2 opposing flows met at some point in the anastomosis and disappeared. Figure 2i shows a sketch of an AAA in which the directions of flow are indicated by arrows. At the meeting point, blood disappeared, apparently sinking into the origin of a penetrating arteriole, which, in most cases, could not be seen from above without the use of FITC-labeled RBCs; this may be the reason why such paradoxical flow has been missed in the past. When the passage of blood into the hole was closely examined, there was as if the two flows were separated by an imaginary membranous wall, which moved left or right depending on the relative flow strengths. In general, AAAs form a peripheral part of cerebral arteries, with penetrating arterioles in the form of T-junctions to supply blood to tissue. Some of these T-junctions are dually fed from two cerebral arteries, and we termed these confluent T-junctions. Most anastomoses were found to have 2 or 3 T-junctions (Figure 2i and 2ii), of which only one served as the confluent T-junction while the remaining junctions served as usual penetrating arterioles. Our observations revealed that even under control conditions, a confluent T-junction could relocate along an AAA from one penetrating arteriole to another (as shown in Figure 2ii). During such relocation, there appeared to be no significant diametric change of any part of the connecting arteriolar branches.

Wall Shear Rate of Blood in AAA

Flow magnitudes were estimated from velocity values of FITC-labeled RBCs multiplied by the cross-sectional area of the vessel. When RBC flow velocity through a vessel with a radius of approximately 0.012 mm (see above) was approximately 2.6 mm/s (see below), the wall shear rate of blood in AAA calculated with Equation 1 was approximately 80/s. However, the shear rate value was found to vary depending on the location of anastomosis. Strangely, it tended to be lower in the proximal parts of connecting branches of the MCA and ACA than around the meeting point, whose diameter tended to be larger. A large variation in flow through connecting arterial branches along T-junctions was a common observation even under physiological conditions. In general, velocity changes in the microvasculature, especially in venules, seemed to be completely unpredictable from diametric changes of vessels.

Hemodynamic and Microvascular Changes Before and After MCAO

Hemodynamic and Hemorheological Changes in AAA and Tissue

When the mouse brain was subjected to ischemia by occluding the left MCA,[10] the flow balance in AAAs was immediately disrupted. Both acute and chronic adaptive hemodynamic changes followed. Acutely, the blood flow velocity in arterioles peripheral to the occluded site dramatically decreased until the flow momentarily came to a full stop (Figure 2iii). However, after a "hesitation" period of a minute or more, retrograde blood flow (Figure 2iv) appeared in the MCA branch (M1) (Figure 3A and 3B). The occurrence of the retrograde flow in this particular branch (M1) was statistically significant ($P<0.05$, in 7 cases of 8). At the same time, flow in another MCA branch (M2) started in the original direction. In general, the flow peripheral to the occlusion site slowed down and various degrees of flow decrease were observed. Increasing viscosity of blood with decreasing flow (non-Newtonian character)[9] means that hemodynamic changes cannot be predicted from Poiseuille law,[9] which assumes the blood viscosity is constant. In 2 cases, RBC aggregates (red) and clot formation (white) stalled blood flow on the MCA side of the AAA. In the capillary network, MCAO induced immediate disappearance of RBCs in the core of the ischemic region, probably caused by a sieving effect, and also to a lesser extent in the marginal zone near the AAA. On the other hand, blood flow near the ACA side of the AAA was rather well preserved. We next compared RBC velocity changes in penetrating branches connecting to the confluent T-junction and those in other penetrating branches of the proximal part of the MCA supplying the ischemic core. After MCAO, RBC velocity change in the T-junction was from 2.6 ± 0.6 mm/s to 2.4 ± 0.9 mm/s, whereas in the penetrating branches of proximal MCA, the RBC velocity decreased sharply from 2.6 ± 1.2 mm/s to 1.1 ± 0.6 mm/s (statistically significant; $P<0.005$, $n=8$).

AAAs, Vascular Remodeling, and Angiogenesis

Microvascular remodeling centering on AAAs in the ischemic tissue after MCAO was preliminarily examined by means of repeated observation every day for a week. Days 0 to 1 (Figure 4A): Capillaries became invisible within a few hours after MCAO, and thereafter there was no RBC passage in the ischemic core. Days 1 to 2 (Figure 4B): Fragments of microvessels and tissue debris were seen, accompanied with massive macrophage infiltration. The macrophages were accidentally made visible by phagocytosed RITC dye which had leaked into the tissue through the disrupted BBB. The dye had originally been injected to visualize the capillary architecture. Day 3 (Figure 4C): Development of new vessels,

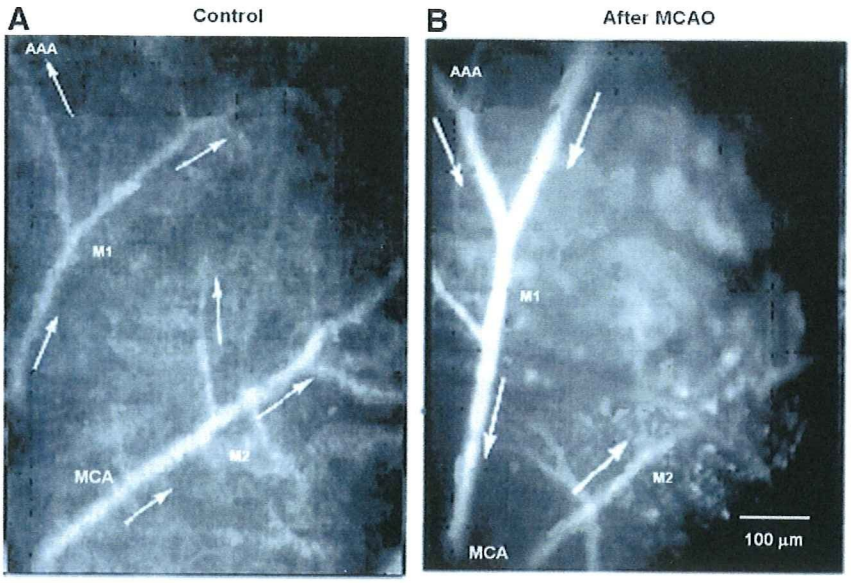

Figure 3. A, Direction of blood flow in M1 was from bottom (MCA stem) to top (periphery) in the control state (before MCAO). B, After MCAO the blood flow reversed from top to bottom; apparently blood was supplied from the ACA via the AAA. The blood changed direction at the branching site of M2 and was supplied to MCA territory.

mostly immature capillaries and reconstructed veins, was seen around the marginal zone of the infarction. Figure 5 shows newly developed straight capillaries (angiogenesis), sprouted from the arteriolo-arteriolar cut end, that connected with dilated and tortuous vessels, remodeled veins and a reactive region of the veins with many modular protrusions. By this stage, labeled RBCs started to flow in capillaries only in the marginal area and remodeled veins, showing unsteady motions. Figure 5 presents a trace of one RBC traveling through new microvasculature in the sequence arteriole-new straight capillary-unidentified channel and reconstructed vein. Day 7: Revascularization similar to that reported by Tomita et al[8] was observed in cerebral ischemic tissue at the 7th day after MCAO in mice. In our experiments, all 8 mice survived 7 days although the ischemic core appeared to be liquefied. In short, angiogenesis was already apparent in the marginal zone at day 3 after MCAO in mice.

Discussion

When blood flow decreases the blood tends to be viscous undergoing transformation to a non-Newtonian fluid, in which lower shear rate results in higher viscosity (η).[9,11,12,13] Under these circumstances, the pressure-flow relationship becomes modified with an additional pressure drop attributable to viscous dissipation.[13]

$$\Delta P = A\eta Q + B\rho Q^2 \quad (2)$$

where A and B are geometric factors determined by the shape of the vessels, ΔP is the perfusion pressure drop, and ρ the fluid density.[13] The vascular diametric control of flow becomes less effective. This viscosity change has to be taken into consideration in flow changes in AAA. On MCAO, the blood flow in the vessels downstream from the occluded site and penetrating arteriole from AAA decreases greatly. Surface of endothelial cells in the peripheral vessels changes from anticoagulant to procoagulant in character,[14,15] and water leaks from blood into the tissue,[16] resulting in hemoconcentration and tissue edema. Capillary RBC flow is greatly disturbed in association with neuronal depolarization (see Tomita et al, available from Nature Preceedings http://precedings.nature.com/documents/3220/version/1). However, there are also some unknown positive factors derived

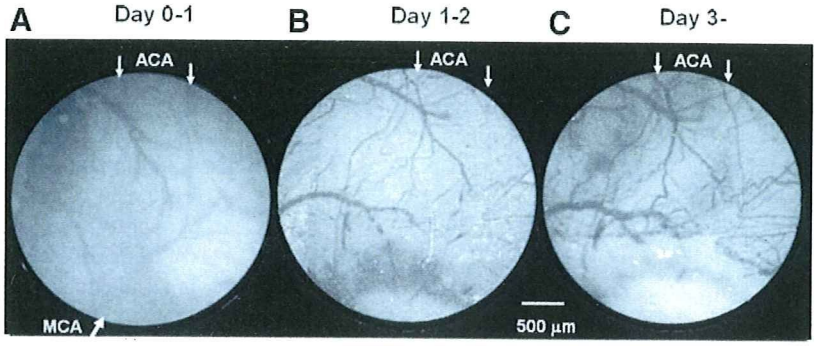

Figure 4. Changes in microvascular geometry in the ROI after MCA occlusion. A, On day 0, small vessels and capillaries peripheral to the MCA became blurred, with destruction of vessel structure. The ischemic core (bottom area) appeared as if it was covered with a dark curtain. Top arrows indicate branches of ACA and bottom MCA. B, On day 2, the "curtain" was lifted and an amorphous white infarct area could be seen. The surrounding area was infiltrated with macrophages, apparently scavenging debris. Fragments of vessels were seen. C, On day 3, revascularization developed in the area surrounding the infarction. New straight capillaries formed by angiogenesis were seen to sprout from the cut end of the MCA branch (arrow). The MCA stem appeared to melt away in B and C.

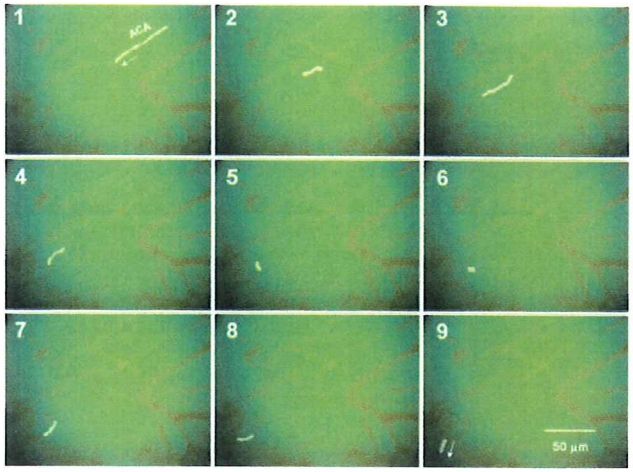

Figure 5. Microphotograph showing new vessels (angiogenesis) and remodeled vessels, enlarged from that used for Figure 4. Note the peculiar shapes of remodeled veins, with bulging and winding corresponding to immature microvasculature. The route traveled by a FITC-labeled RBCs from an arteriole of the MCA through a newly developed straight capillary to a vein is shown, frame by frame every 1/30 s: 1, arteriole of ACA; 2 to 4, newly developed straight capillaries; 5 to 9, vein. The length of elongation is broadly related to the RBC velocity.

from active or surviving nondepolarized neurons that might facilitate capillary RBC velocity.[17] The blood flow in the ischemic tissue is just unknown.

The FITC-labeled RBC method[7] used in the present study provides a unique tool to investigate the direction and magnitude of blood flow in AAAs in situ, not only in physiological but also in ischemic circumstances, because the use of such FITC-labeled RBCs has made it possible to trace directly blood movements and blood flow directions that would otherwise be undetectable. We found that blood was flowing into some AAAs from both the ACA and MCA, which seemed paradoxical but could be understood in terms of the concept of the confluent T-junction. The AAA region was sometimes called the watershed area, because the perfusion pressure was supposed to be lowest,[18] and multiple occlusions were largely interpreted as thrombi secondary to slowing of the blood flow or attributable to microemboli.[19] However, by tracing FITC-labeled RBCs, we found that the AAA and T junctions were well perfused in the normal state, because they were dually supplied from both the MCA and ACA. In the present study, we were not able to detect any diametric changes of the AAA channel even when the blood reversed its direction of flow. Interestingly, the locus of the dually fed T-junction was not fixed, but could move apparently spontaneously along the AAA. Theoretically, the pressure along the ACA segment of the AAA and the pressure along the MCA segment of the AAA will eventually be equal at some locus within the AAA. The site where the pressure is equal will move to a particular penetrating arteriole where the downstream resistance results in the best match for pressure equilibration. Although the penetrating arteriole is fed from both directions, the ratio will not necessarily to be fifty-fifty, because the flow required from one particular direction may need to be greater than that from the opposite direction to achieve the pressure drop necessary for the pressure to be equal at the actual T-junction. The fact that the locus moved dynamically, as observed in this article, is therefore not entirely unexpected, because slight changes in resistance downstream from a particular penetrating arteriole and slight changes in the pressure drop selectively across the MCA or ACA are bound to occur. This would change the locus of best match for pressure equilibration—a complicated regulatory mechanism of vis a tergo and vis a fronte forces. On MCAO, we observed a brief "hesitation" of blood flow in the MCA side of AAA. Immediately after the occlusion, blood flow in the downstream region stopped, which would result in a momentary increase in the blood viscosity. It is of interest to note that the shear rate of blood flowing through the AAA was approximately 80^{-s} in the control state. This is the critical threshold below which the blood tends to behave as a non-Newtonian fluid. Because there was no significant diametric change of the channel at the time of occlusion, hemorheological factors of the blood per se in the vessels, such as the increased viscosity, may govern the hemodynamic flow changes. If zero flow or low flow persisted, it might cause severe infarction.[20] However, Shih et al[21] reported active dilation of penetrating arterioles leading to restoration of red blood cell flux to the penumbral neocortex after focal stroke. Maeda et al[22] found that larger anastomoses in angiotensinogen-knockout mice attenuate early metabolic disturbances after MCAO. The penetrating arterioles presumably respond to peripheral requirement by providing blood to the area via a vis a fronte. Flow would restart if the pressure gradient exceeded the yield point of the RBC aggregates, and the patent AAA would supply blood through collateral channels to the acutely ischemic territories (so-called ischemic penumbra). The MCA branch would also supply blood to the MCA territories retrogradely from the ACA via small diameter to larger diameter arterioles. We observed in all cases studied that blood flow was redistributed to other MCA branches. For the efficient functioning of AAA, 2 points seem to be important: blood in the AAA channel must be kept flowing, and the channel wall must be strong enough preventing vessels from collapse. The latter could be the reason for the ampoule shape, whose diameter was larger than that of the orifice of the AAA. The T-junctions in AAA thus served as a center of collateral channels to rescue the ischemic area, and this occurred within minutes after MCAO, determining the fate of the ischemic tissue.

During successive daily observations of the same microvasculature of the mouse cortex, we noticed the appearance of new vessels, consisting mostly of immature capillaries and peculiarly shaped veins, remodeled around the marginal zone of the infarction, by day 3. RBCs were already flowing through the new capillaries and remodeled veins with unsteady motions, presumably providing oxygen to the penumbral region. On the other hand, in the ischemic core RBCs disappeared from the capillary network from the beginning of ischemia, provoking immediate, severe tissue anoxia, because RBCs carry much more oxygen than plasma. Capillaries were destroyed, and the ischemic core became liquefied.

Sources of Funding

This work was supported by JSPS Grant-in-Aid #17390255 and #19591008. We thank Otsuka Pharmaceutical Co Ltd. Pfizer Japan Inc. and Novartis Pharma K.K. for their financial support.

Disclosures

None.

References

1. Mchedlishvili G. *Arterial Behavior and Blood Circulation in the Brain.* New York: Plenum Press; 1986:130–135.
2. Coyle P, Jokelainen PT. Dorsal cerebral arterial collaterals of the rat. *Anat Rec.* 1982;203:397–404.
3. Liebeskind DS. Collateral circulation. *Stroke.* 2003;34:2279–2284.
4. Adams RD, Van der Eecken HM. Vascular diseases of the brain. *Annu Rev Med.* 1953;4:213–252.
5. Gannushkina IV, Baranchikova MV, Shinkarenko VS, Komm SG. Status of the "dead point" of blood flow in anastomoses of superficial cerebral arteries as affected by an acute increase of blood pressure. *Biull Eksp Biol Med.* 1987;104:548–552.
6. Seylaz J, Charbonne' R, Nanri K, von Euw D, Borredon J, Kacem K, Meric P, Pinard E. Dynamic in vivo measurement of erythrocyte velocity and flow in capillaries and of microvessel diameter in the rat brain by confocal laser microscopy. *J Cereb Blood Flow Metab.* 1999;19: 863–870.
7. Tomita M, Osada T, Schiszler I, Tomita Y, Unekawa M, Toriumi H, Tanahashi N, Suzuki N. Automated method for tracking vast numbers of FITC-labeled RBC's in microvessels of rat brain in vivo using a high-speed confocal microscope system. *Microcirculation.* 2008:15: 163–174.
8. Tomita Y, Kubis N, Calando Y, Tran Dinh A, Meric P, Seylaz J, Pinard E. Long-term in vivo investigation of mouse cerebral microcirculation by fluorescence confocal microscopy in the area of focal ischemia. *J Cereb Blood Flow Metab.* 2005:25:858–867.
9. Tomita M. Blood flow control in the brain: possible biphasic mechanism of functional hyperemia (review). *Asian Biomedicine.* 2007;1:17–31.
10. Tamura A, Graham DI, McCulloch J, Teasdale GM. Focal cerebral ischaemia in the rat: Description of technique and early neuropathological consequences following middle cerebral artery occlusion. *J Cereb Blood Flow Metab.* 1981;1:53–60.
11. Tomita M. Basic mechanisms of brain ischemia (Minireview on microcirculation), Capillo-venous flow disturbances in brain ischemia. In: Erdo F, ed. *Recent Advances and New Strategies in Stroke Research,* Transworld Research Network. 37/661 (2), Port P.O., Trivandrum-695 023, India: Kerala; 2008:91–112.
12. Tomita M. Microcirculatory stasis in the brain (Presidential Address). In: Tomita M, Mchedlishvili G, Rosenblum WI, Heiss W-D, Fukuuchi Y, eds. *Microcirculatory Stasis in the Brain,* Amsterdam: Excerpta Medica, ICS 1031; 1993:1–7.
13. Chien S. Present state of blood rheology. In: Messmer K, Schmid-Schönbein H, eds. *Hemodilution,* Basel: Kager; 1972:1–45.
14. Hallenbeck JM, Dutka AJ. Background review and current concepts of reperfusion injury. *Arch Neurol.* 1990;47:1245–1254.
15. Mchedlishvili G, Tomita M, Schmid-Schönbein GW. Hemorrheology in microcirculation: Pathological changes (Internet Virtual Symposium, The 7th Tbilisi Symposium), *Keio J Med.* 2000;49(Suppl 3):1–82 (Available from http://mtomita.jp/content.htm).
16. Tomita M. Increased intracranial pressure and brain edema. In: Kalimo H, ed. Pathology & Genetics, Structure and functions of CNS blood vessels, *Cerebrovascular Diseases,* ISN Book Series, Basel: ISN Neuropath Press; 2005:39–49.
17. Akgoren N, Lauritzen M. Functional recruitment of red blood cells to rat brain microcirculation accompanying increased neuronal activity in cerebellar cortex. *Neuroreport.* 1999;10:3257–3263.
18. Naritomi H, Sawada T, Kuriyama Y, Kinugawa H, Kaneko T, Takamiya M. Effect of chronic middle cerebral artery stenosis on the local cerebral hemodynamics. *Stroke.* 1985:16:214–219.
19. Torvik A. The pathogenesis of watershed infarcts in the brain. *Stroke.* 1984:15:221–223.
20. Jorgensen L, Torvik A. Ischaemic cerebrovascular diseases in an autopsy series. 2. Prevalence, location, pathogenesis, and clinical course of cerebral infarcts. *J Neurol Sci.* 1969;9:285–320.
21. Shih AY, Friedman B, Drew PJ, Tsai PS, Lyden PD, Kleinfeld D. Active dilation of penetrating arterioles restores red blood cell flux to penumbral neocortex after focal stroke. *J Cereb Blood Flow Metab.* 2009;29: 738–751.
22. Maeda K, Hata R, Bader M, Walther T, Hossmann KA. Larger anastomoses in angiotensinogen-knockout mice attenuate early metabolic disturbances after middle cerebral artery occlusion. *J Cereb Blood Flow Metab.* 1999;19:1092–1098.

BRAIN RESEARCH 1320 (2010) 69–73

available at www.sciencedirect.com

www.elsevier.com/locate/brainres

BRAIN RESEARCH

Research Report

RBC velocities in single capillaries of mouse and rat brains are the same, despite 10-fold difference in body size

Miyuki Unekawa[a], *Minoru Tomita*[a], *Yutaka Tomita*[a], *Haruki Toriumi*[a], *Koichi Miyaki*[b,1], *Norihiro Suzuki*[a,*]

[a]*Department of Neurology, School of Medicine, Keio University, 35 Shinanomachi, Shinjuku-ku, Tokyo 160-8582, Japan*
[b]*Department of Preventive Medicine for Cerebrovascular Disease, School of Medicine, Keio University, 35 Shinanomachi, Shinjuku-ku, Tokyo 160-8582, Japan*

ARTICLE INFO

Article history:
Accepted 12 January 2010
Available online 18 January 2010

Keywords:
Frequency distribution function
Microcirculation
Mouse
RBC velocity
Cerebral cortex

ABSTRACT

Employing high-speed camera laser-scanning confocal microscopy with RBC-tracking software, we previously showed that RBC velocities in intraparenchymal capillaries of rat cerebral cortex are distributed over a wide range. In the present work, we measured RBC velocities in mice, whose body weights are less than one-tenth of that of rats. In an isoflurane-anesthetized mouse, a cranial window was opened in the left temporo-parietal region. Intravenously administered FITC-labeled RBCs were automatically recognized and tracked frame-by-frame at 500 fps, and the velocities of all RBCs recognized were calculated with our Matlab-domain software, KEIO-IS2. Among 15241 RBCs detected in the ROI in 21 mice, 1655 were identified as flowing in capillaries. The velocities of these RBCs ranged from 0.15 to 8.6 mm/s, with a mean of 2.03 ± 1.42 mm/s. A frequency distribution plot showed that RBC velocities were clustered at around 1.0 mm/s, tailing up to 8.6 mm/s, and 59% of the RBCs in capillaries showed velocities within the range of 0.5 to 2.0 mm/s. Unexpectedly, these characteristics of RBC velocities in mice were very similar to those of rats, despite differences in RBC diameter (6.0 vs. 6.5 μm), body size (25 vs. 327 g), heart rate (461 vs. 319 bpm) and arterial blood pressure (86 vs. 84 mm Hg). We speculate that physical factors relating to oxygen exchange may constrain general RBC velocity in capillaries to a certain range for optimum oxygen exchange, regardless of species.

1. Introduction

Red blood cells (RBCs) in single capillaries play a critical role in supplying neurons with oxygen, but literature values of their velocity are quite discrepant. Two-slit photometry and cross-correlation (Ma et al., 1974), high-speed microcinephotography (Pawlik et al., 1981), intravital microfilming (Ivanov et al., 1981), radioactive microspheres (Chang et al., 1984), a dual window technique with two fluorescent tracers (Yamaguchi et al., 1992), a dual window and cross-correlation method

* Corresponding author. Fax: +81 3 3353 1272.
E-mail address: nrsuzuki@sc.itc.keio.ac.jp (N. Suzuki).

Abbreviations: CBF, cerebral blood flow; FITC, fluorescein isothiocyanate; fps, frames per second; RBC, red blood cell; ROI, region of interest

[1] Present address: Division of Genomic Epidemiology, Department of Clinical Research and Informatics, International Medical Center of Japan, Tokyo, Japan.

0006-8993/$ – see front matter © 2010 Elsevier B.V. All rights reserved.
doi:10.1016/j.brainres.2010.01.032

(Hudetz, 1997a), laser-scanning confocal fluorescence microscopy (Seylaz et al., 1999) and two-photon laser-scanning microscopy (Hutchinson et al., 2006) have been employed to measure RBC velocity in microvessels of cerebral cortex of various species. The reported mean velocities center around 1 mm/s, with a range of 0.39 to 2.08 mm/s.

In previous communications, we have reported the detection of RBCs having much higher velocity than the above literature values in urethane-anesthetized rats, using a laser-scanning confocal microscope system with Matlab-domain tracking software, KEIO-IS2, developed by us (Schiszler et al., 2005; Tomita et al., 2008; Unekawa et al., 2008). The use of a high-speed camera (500 frames/s (fps)) was crucially important, since RBCs with relatively high velocities would have been missed in successive frames and would therefore have been uncounted in previous methods which employed conventional cameras with low frame rates (for example, 30 fps).

Recently, there has been a shift in animal experiments from the use of rats to mice, since the latter have a smaller body size and are convenient for the development of gene-recombination technologies. In the present work, we aimed to measure the velocities of RBCs in single capillaries in the mouse brain for comparison with those in rats, and further, to examine the characteristics of the RBC motion, including the frequency distribution function and fluctuations of RBC velocity in single capillaries.

2. Results

The body weight of mice is about one-tenth of that of rats (average body weight of the mice we used was 26.3±3.1 g, versus 327±32 g for Wistar rats). The diameter of mouse RBCs was slightly smaller (6.0 μm) than that of rat RBCs (6.5 μm) (unpublished observation with a VEC–DIC microscope). The heart rate of mice at the beginning of experiments was statistically significantly higher (461.4±50.5 bpm) than that of rats measured with the same apparatus (314.5±50.6 bpm) ($p<0.001$), although arterial blood pressures were similar (85.7±23.7 mm Hg in mice and 83.5±13.7 mm Hg in rats). Arterial blood pressure and heart rate were stable during the experiments.

In 21 mice, 726±614 RBCs per mouse (ranging from 72 to 1444) were detected as moving RBCs and 79±82 RBCs per mouse (ranging 5 to 262) were identified as flowing in single capillaries during the recording period (10 s) in the region of interest (ROI) of 500×500 μm. The total number of capillaries identified according to our criteria (see Experimental procedures) was 9.1±8.9 (per mouse, ranging 1 to 36) and the sum of the length of the detected capillaries was 635±563 μm per mouse (ranging 70 to 2320 μm). These numbers were similar to those of rats used in the previous experiments (Unekawa et al., 2008); namely, the measurement conditions and selected ROIs seem to be well matched in the different experiments.

As shown in Fig. 1, mean RBC velocity in single capillaries in each mouse was 2.16±1.31 mm/s with a range of 0.76 (minimum value) to 6.57 mm/s (maximum value). The mean velocity was not statistically significantly different from that in rats (2.20±1.59 mm/s, with a range of 0.93 to 4.06 mm/s).

The frequency distribution function of RBC velocities (h(v)) was obtained by stratifying velocity at every 0.5 mm/s and

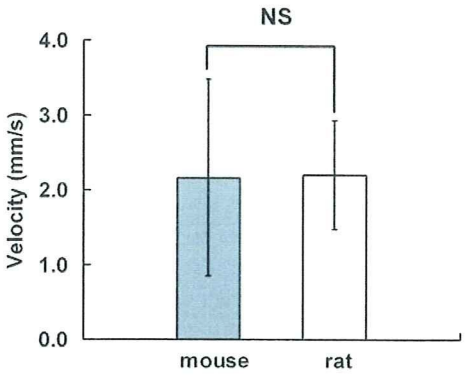

Fig. 1 – RBC velocity in single capillaries in mice (shadowed column, $n=21$) and rats (open column, $n=37$). Values are represented as mean±SD. The velocities in the two species were not significantly different ($p>0.05$). The values of rat RBC velocity are those reported previously (Unekawa et al., 2008).

counting the number of RBC appearances in the strata after integration of all RBC velocity data collected in a single capillary (Fig. 2). The total number of RBCs in capillaries was 1655 among the total of 15 241 RBCs detected in all categories of vessels (arterioles, capillaries and venules) in the present experiments. The mean velocity of RBCs exclusively in single capillaries was 2.03±1.42 mm/s. This value was not statistically significantly different from the value in rats ($p>0.05$), even when we employed Mann–Whitney's U test or t-test after logarithmic conversion (the distribution curve was not a normal probability distribution). RBC velocities in capillaries were clustered at around 1.0 mm/s, tailing to higher velocities of up to 8.6 mm/s, and 59% of the RBCs in capillaries showed a velocity within the range of 0.5 to 2.0 mm/s. Moment analysis of the frequency distribution functions plotted against velocity (h(v)) in mice and rats revealed that the 4th moment,

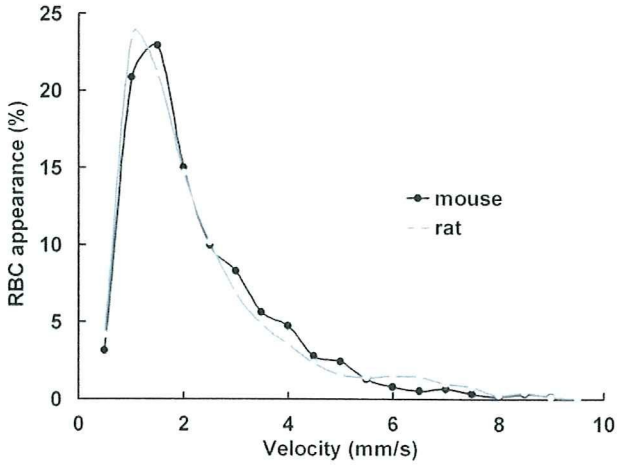

Fig. 2 – Frequency distribution function of RBC velocities in single capillaries in mice (closed circles and black lines, total number of RBCs=1655) and in rats (open circles and gray lines, total number of RBCs=4311). Each plot is shown as a percentage with respect to the total number of RBCs. The values of rat RBC velocity are those reported previously (Unekawa et al., 2008).

kurtosis, was 2.97 for mice and 2.78 for rats, respectively. The similarity of these higher moments further supports the similarity of the two curves.

We have demonstrated that capillary RBC velocity fluctuates temporally and spatially, and yet each capillary has a characteristic velocity (Unekawa et al., 2008). When capillaries in which RBCs were detected at least 5 times were selected, 1360 RBCs were obtained as flowing in 80 capillaries. The mean velocities of RBCs were calculated for the individual capillaries, and plotted as short horizontal bars with small dots representing each velocity (Fig. 3). The mean and standard deviation of the individual mean velocities in single capillaries were 1.76± 0.59 mm/s, again being not significantly different from those of rats (1.96±1.26 mm/s; previously presented data (Unekawa et al., 2008)). The average of the SD of RBC velocities in each capillary, a surrogate indicator of the individual fluctuations, was 0.34 mm/s (35.6% of the mean value), and this is also not significantly different from the average value of 0.59 mm/s (34.0%) in rats. It appears that RBC velocities in capillaries continually fluctuate within a limited range. The fluctuation was specific to individual capillaries, as was the case in rats.

3. Discussion

The present results demonstrate that the movements of RBCs in single capillaries in mice are quite similar to those in rats, notwithstanding the differences in RBC diameter, body size and heart rate. The average RBC velocity in mice is much faster than the previously reported value in intact capillaries of mouse cerebral cortex (0.53 mm/s) (Tomita et al., 2005) or in normal capillaries or neocapillaries generated on gel–nylon mesh (0.7–1.3 mm/s)(Nageswari et al., 2002; Niimi et al., 2000). This difference is considered to be due to the difference of frame rate or shutter speed of the camera in the recording system (30 fps in the literature vs 500 fps in the present experiments). Actually, RBC velocities of 1.1–2.08 mm/s were observed with a high frame rate (200–400 fps) in cats (Chang et al., 1984; Pawlik et al., 1981; Yamaguchi et al., 1992). We previously reported that there is a clear frame rate dependency of apparent RBC velocity; when higher frame rates are employed, higher mean RBC velocities are obtained, because rapidly moving RBCs can only be detected when a high-speed camera is used for analysis (Unekawa et al., 2008). Namely, rapidly moving RBCs are missing in successive frames at low frame rates, and are therefore uncounted. The lower values in the literature were all acquired at low frame rates.

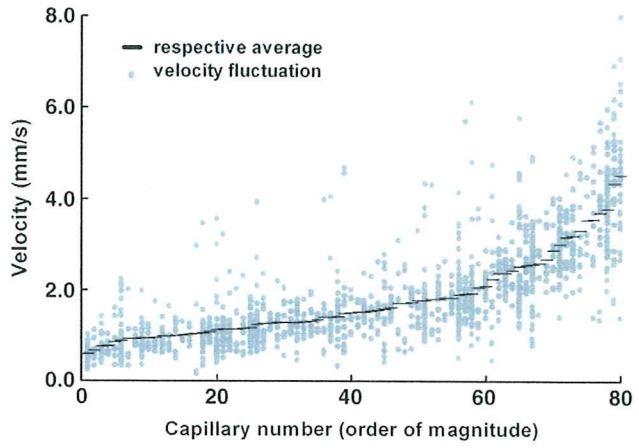

Fig. 3 – Fluctuation (gray dots) and respective averages (horizontal small bars) of RBC velocities in individual capillaries. Eighty capillaries, in which RBC tracks were detected 5 or more times, were selected in 21 mice and ranked in order of their average velocities. All fluctuating velocities were plotted against rank.

It may be thought that similar velocity of RBCs reflects a similar cerebral blood flow (CBF) in rodents. Absolute assessment of local CBF has been achieved by means of a ^{14}C-iodoantipyrine autoradiographic technique. Local CBF in the cerebral cortex under physiological conditions or at an intact site in partially ischemic mice is 70–150 ml/100 g/min (de Vasconcelos et al., 2005; Engel et al., 2008; Jiang et al., 2006; Kawai et al., 1997; Leithner et al., 2008; Lundblad and Bentzer, 2007; Niwa et al., 2001; Saleem et al., 2007), which is slightly higher than that of rats (45–145 ml/100 g/min) (Chi et al., 1999; Miyamoto and Auer, 2000; Narayanan et al., 2002; Takagi et al., 1995; Tanaka et al., 2001; Tohyama et al., 1997). On the other hand, lower CBF (25–50 ml/100 g/min) has been demonstrated in cats (Goadsby, 1989; Sutton et al., 1989). The regular relationship between resting metabolic rate, or rate of oxygen consumption, and the body size of an animal is well known. In most mammals, blood volume is a constant fraction of the body, but RBC size and capillary diameter are constant. In order to satisfy higher oxygen requirement, capillary density must be higher (shorter diffusion distance) in small animals (Schmidt-Nielsen, 1984). Therefore, it is reasonable that blood flow per a gram tissue is higher in small animals. Furthermore, diversity of CBF might be due to strain difference or be influenced by the mode of anesthesia. We used inhalation of isoflurane in mice and intraperitoneal administration of urethane in rats. Nevertheless, the essentially identical velocity characteristics, especially the frequency distribution function, of RBCs in mice and rats seem noteworthy.

The responses of CBF to hypercapnia was much higher than the response of RBC velocity (Hudetz, 1997b). The onset and the peak increases in RBC velocity to neuronal activation in response to hind paw stimulation were not corresponded to those of CBF, suggesting that the capillary and arteriole are controlled by independent mechanisms (Matsuura et al., 1999). Cortical spreading depression induced periodic decreases in both RBC number and velocity until RBCs halted or disappeared (Tomita et al., 2009). RBC velocity in capillaries remained broadly unchanged, whereas RBC number (appearance) decreased by topical application or intravenous administration of nitroprusside, whereas microflow markedly increased (Tomita et al., in press). The area of usual CBF measurement is rather large (for example, 1 mm^3 with laser Doppler flowmetry) and the obtained values are the average in the area containing arterioles, venules, and so on. But our results of RBC velocity are only in capillaries, excluding such vessels. Thus, we consider that RBC velocity in capillaries and CBF are not always regulated by a single or simple mechanism.

Generally, the specific metabolic rate increases as the animal body weight decreases. CBF also scales with body size

as mentioned above. It represents that the smaller the animal, the higher the volume rate of blood flow. Mammalian cerebral blood volume appears to be constant, resulting that mean transit time should decrease with decreasing brain size (Shockley and LaManna, 1988). Therefore, since the RBC velocity distribution of mice is similar with that of rats, the capillary length may be shorter in smaller animals. However, the detected length of capillaries of mice was comparative with that of rats in this experiment. Mean transit time is also proportional to the ratio of blood volume to blood flow, according to Stewart–Hamilton equation. The length of the capillaries, which was identified with Matlab domain KEIO-IS2, and calculated mean transit time in mice were comparative with those in rats in this experiment. Furthermore, similar RBC velocity and increased oxygen consumption may show oxygen delivery is facilitated in the smaller animals.

RBC velocity in cerebrocortical capillaries of other species has been estimated as around 1 mm/s. However, there are methodological difficulties and ethical problems in directly observing capillaries in human brain. Packed RBC volume, red cell size, capillary diameter, blood gases and blood pressure are fairly constant across mammalian species. Scaling lows of the complex branching pattern and vascular tree structure have been shown to be deduced on the basis of the minimum energy hypothesis and conservation of energy under steady state conditions (Kassab, 2006). We hypothesize that general RBC velocity in capillaries is limited to a certain range by physical factors related to the requirements for optimum oxygen extraction, regardless of species.

4. Experimental procedures

Twenty-one C57BL/6J mice (8–10 weeks old, body weight, 26.3±3.1 g) were used with the approval (# 071095) of the Animal Ethics Committee of Keio University, and all experimental procedures were in accordance with the university's guidelines for the care and use of laboratory animals. Under anesthesia with isoflurane (ca. 1.5%) administered via a concentration-controllable anesthesia unit (400, Univentor Ltd., Zejtun, Malta), each mouse was fixed to a head-holder and a cranial window of approximately 3 mm in diameter was opened in the left side of the skull at the parieto-temporal region of the cerebral cortex. The dura was kept intact and the exposed cortex was covered with a cover slip to prevent it from drying out. A tail vein was catheterized to intravenously inject various solutions. An appropriate capillary-rich ROI in the cerebral cortex was selected, and 0.05 ml of fluorescein isothiocyanate (FITC)-labeled RBC suspension, prepared beforehand according to Seylaz et al. (Seylaz et al., 1999), was injected into the bloodstream through the venous catheter. Fall of body temperature was prevented with a heating-pad and thermo-controller (BWT-100, Bioresearch Center Co., Ltd., Nagoya, Japan). In some experiments, arterial blood pressure and heart rate were recorded with an intermittent cuff method applied to the hindlimb (a non-invasive blood pressure monitor; MK-200, Muromachi Kikai Co., Ltd., Tokyo, Japan). The methods of measurement of RBC velocity using the high-speed camera (500 fps) laser-scanning confocal fluorescence microscope and the image analyzing system with a MATLAB® (The Math Works, Inc., Natick, MA, USA) environment with application software (KEIO-IS2) developed in our laboratory (Schiszler et al., 2005) were reported elsewhere (Tomita et al., 2008; Unekawa et al., 2008). With reference to the alternatively recorded images obtained using a conventional video camera, we defined single capillaries as having a diameter less than 10 μm, based on other reports (Hutchinson et al., 2006; Williams et al., 1993). The frequency distribution function was obtained by stratification of velocities at every 0.5 mm/s and counting the appearance of RBCs within the range. The characteristics of RBC velocities in mice were compared with reported data for rats (Unekawa et al., 2008).

Data in text and figures are presented as mean±standard deviation (SD). Non-paired Student's *t*-test was performed to assess statistical significance, except where otherwise noted in the text.

Acknowledgments

The authors thank Prof. Susumu Terakawa (Photon Medical Research Center, Hamamatsu University School of Medicine, Japan) for determination of the size of RBCs. This work was supported by JSPS Grant-in-Aid # 17390255 (Suzuki, N) and # 19591008 (Tomita, Y). The authors also thank Otsuka Pharmaceutical Co., Ltd., Novartis Pharma K.K. and Pfizer Japan Inc. for financial supports.

REFERENCES

Chang, B.L., Santillan, G., Bing, R.J., 1984. Red cell velocity and autoregulation in the cerebral cortex of the cat. Brain Res. 308, 15–24.

Chi, O.Z., Chang, Q., Wang, G., Liu, X., Weiss, H.R., 1999. A nonNMDA antagonist, GYKI 52466 improves microscopic O_2 balance in the cortex during focal cerebral ischemia. Neurol. Res. 21, 299–304.

de Vasconcelos, A.P., Bouilleret, V., Riban, V., Wasterlain, C., Nehlig, A., 2005. Role of nitric oxide in cerebral blood flow changes during kainate seizures in mice: genetic and pharmacological approaches. Neurobiol. Dis. 18, 270–281.

Engel, D.C., Mies, G., Terpolilli, N.A., Trabold, R., Loch, A., De Zeeuw, C.I., Weber, J.T., Maas, A.I., Plesnila, N., 2008. Changes of cerebral blood flow during the secondary expansion of a cortical contusion assessed by ^{14}C-iodoantipyrine autoradiography in mice using a non-invasive protocol. J. Neurotrauma 25, 739–753.

Goadsby, P.J., 1989. Effect of stimulation of facial nerve on regional cerebral blood flow and glucose utilization in cats. Am. J. Physiol. 257, R517–R521.

Hudetz, A.G., 1997a. Blood flow in the cerebral capillary network: a review emphasizing observations with intravital microscopy. Microcirculation 4, 233–252.

Hudetz, A.G., 1997b. Regulation of oxygen supply in the cerebral circulation. Adv. Exp. Med. Biol. 428, 513–520.

Hutchinson, E.B., Stefanovic, B., Koretsky, A.P., Silva, A.C., 2006. Spatial flow-volume dissociation of the cerebral microcirculatory response to mild hypercapnia. Neuroimage 32, 520–530.

Ivanov, K.P., Kalinina, M.K., Levkovich Yu, I., 1981. Blood flow velocity in capillaries of brain and muscles and its physiological significance. Microvasc. Res. 22, 143–155.

Jiang, W., Gu, W., Hossmann, K.A., Mies, G., Wester, P., 2006. Establishing a photothrombotic 'ring' stroke model in adult mice with late spontaneous reperfusion: quantitative

measurements of cerebral blood flow and cerebral protein synthesis. J. Cereb. Blood Flow Metab. 26, 927–936.
Kassab, G.S., 2006. Scaling laws of vascular trees: of form and function. Am. J. Physiol. Heart Circ. Physiol. 290, H894–H903.
Kawai, N., Keep, R.F., Betz, A.L., 1997. Hyperglycemia and the vascular effects of cerebral ischemia. Stroke 28, 149–154.
Leithner, C., Gertz, K., Schrock, H., Priller, J., Prass, K., Steinbrink, J., Villringer, A., Endres, M., Lindauer, U., Dirnagl, U., Royl, G., 2008. A flow sensitive alternating inversion recovery (FAIR)-MRI protocol to measure hemispheric cerebral blood flow in a mouse stroke model. Exp. Neurol. 210, 118–127.
Lundblad, C., Bentzer, P., 2007. Effects of L-arginine on cerebral blood flow, microvascular permeability, number of perfused capillaries, and brain water content in the traumatized mouse brain. Microvasc. Res. 74, 1–8.
Ma, Y.P., Koo, A., Kwan, H.C., Cheng, K.K., 1974. On-line measurement of the dynamic velocity of erythrocytes in the cerebral microvessels in the rat. Microvasc. Res. 8, 1–13.
Matsuura, T., Fujita, H., Seki, C., Kashikura, K., Yamada, K., Kanno, I., 1999. CBF change evoked by somatosensory activation measured by laser-Doppler flowmetry: independent evaluation of RBC velocity and RBC concentration. Jpn. J. Physiol. 49, 289–296.
Miyamoto, O., Auer, R.N., 2000. Hypoxia, hyperoxia, ischemia, and brain necrosis. Neurology 54, 362–371.
Nageswari, K., Yamaguchi, S., Yamakawa, T., Niimi, H., 2002. Quantitative assessment of cerebral neocapillary network and its remodeling in mice using intravital fluorescence videomicroscopy. Angiogenesis 5, 99–105.
Narayanan, U., Weiss, H.R., Liu, X., Chi, O.Z., 2002. Exogenous endothelin-1 improves microvascular oxygen balance during focal cerebral ischemia in the rat. Regul. Pept. 105, 1–7.
Niimi, H., Nageswari, K., Ranade, G., Yamaguchi, S., Yamakawa, T., 2000. Microcirculatory characterization of cerebral angiogenesis in mice using intravital videomicroscopy. Clin. Hemorheol. Microcirc. 23, 293–301.
Niwa, K., Haensel, C., Ross, M.E., Iadecola, C., 2001. Cyclooxygenase-1 participates in selected vasodilator responses of the cerebral circulation. Circ. Res. 88, 600–608.
Pawlik, G., Rackl, A., Bing, R.J., 1981. Quantitative capillary topography and blood flow in the cerebral cortex of cats: an in vivo microscopic study. Brain Res. 208, 35–58.
Saleem, S., Li, R.C., Wei, G., Dore, S., 2007. Effects of EP1 receptor on cerebral blood flow in the middle cerebral artery occlusion model of stroke in mice. J. Neurosci. Res. 85, 2433–2440.
Schiszler, I., Takeda, H., Tomita, M., Tomita, Y., Osada, T., Unekawa, M., Tanahashi, N., Suzuki, N., 2005. Software (KEIO-IS2) for automatically tracking red blood cells (RBCs) with calculation of individual RBC velocities in single capillaries of rat brain. J. Cereb. Blood. Flow Metab. 25 (suppl), S541.
Schmidt-Nielsen, K., 1984. Scaling, Why is Animal Size so Important? Cambridge University Press, Cambridge, New York.
Seylaz, J., Charbonné, R., Nanri, K., Von Euw, D., Borredon, J., Kacem, K., Méric, P., Pinard, E., 1999. Dynamic in vivo measurement of erythrocyte velocity and flow in capillaries and of microvessel diameter in the rat brain by confocal laser microscopy. J. Cereb. Blood Flow Metab. 19, 863–870.
Shockley, R.P., LaManna, J.C., 1988. Determination of rat cerebral cortical blood volume changes by capillary mean transit time analysis during hypoxia, hypercapnia and hyperventilation. Brain Res. 454, 170–178.
Sutton, L.N., Barranco, D., Greenberg, J., Dante, S., Florin, S., Welsh, F., 1989. Cerebral blood flow and glucose metabolism in experimental brain edema. J. Neurosurg. 71, 868–874.
Takagi, K., Zhao, W., Busto, R., Ginsberg, M.D., 1995. Local hemodynamic changes during transient middle cerebral artery occlusion and recirculation in the rat: a [^{14}C]iodoantipyrine autoradiographic study. Brain Res. 691, 160–168.
Tanaka, K., Nogawa, S., Ito, D., Suzuki, S., Dembo, T., Kosakai, A., Fukuuchi, Y., 2001. Phosphorylation of cyclic adenosine monophosphate response element binding protein in oligodendrocytes in the corpus callosum after focal cerebral ischemia in the rat. J. Cereb. Blood Flow Metab. 21, 1177–1188.
Tohyama, Y., Sako, K., Yonemasu, Y., 1997. Protein kinase C in focal ischemic rat brain: dual autoradiographic analysis of [^{14}C] iodoantipyrine (IAP) and [^{3}H]phorbol-12, 13-dibutyrate (PDBu). Brain Res. 750, 155–160.
Tomita, Y., Kubis, N., Calando, Y., Tran Dinh, A., Meric, P., Seylaz, J., Pinard, E., 2005. Long-term in vivo investigation of mouse cerebral microcirculation by fluorescence confocal microscopy in the area of focal ischemia. J. Cereb. Blood Flow Metab. 25, 858–867.
Tomita, M., Osada, T., Schiszler, I., Tomita, Y., Unekawa, M., Toriumi, H., Tanahashi, N., Suzuki, N., 2008. Automated method for tracking vast numbers of FITC-labeled RBCs in microvessels of rat brain in vivo using a high-speed confocal microscope system. Microcirculation 15, 163–174.
Tomita, M., Tomita, Y., Toriumi, H., Unekawa, M., Suzuki, N., 2009. Coupling of capillary RBC flow failure with neuronal depolarization. Nature Proceedings. [The data are available at http://precedings.nature.com/documents/3220/version/1].
Tomita, M., Osada, T., Unekawa, M., Tomita, Y., Toriumi, H., Suzuki, N., in press. Exogenous nitric oxide increases microflow but decreases RBC attendance in single capillaries in rat cerebral cortex. Microvasc. Rev. Commun.
Unekawa, M., Tomita, M., Osada, T., Tomita, Y., Toriumi, H., Tatarishvili, J., Suzuki, N., 2008. Frequency distribution function of red blood cell velocities in single capillaries of the rat cerebral cortex using intravital laser-scanning confocal microscopy with high-speed camera. Asian Biomed. 2, 203–218.
Williams, J.L., Shea, M., Jones, S.C., 1993. Evidence that heterogeneity of cerebral blood flow does not involve vascular recruitment. Am. J. Physiol. 264, H1740–H1743.
Yamaguchi, S., Yamakawa, T., Niimi, H., 1992. Red cell velocity and microvessel diameter measurement by a two fluorescent tracer method under epifluorescence microscopy: application to cerebral microvessels of cats. Int. J. Microcirc. Clin. Exp. 11, 403–416.